Synthetic Molybdenum-Iron-Sulfur Clusters. Preparation, Structures, and Properties of the $[S_2MoS_2Fe(SC_6H_5)_2]^{2-}$ and $[S_2MoS_2FeCl_2]^{2-}$ Ions

R. H. Tieckelmann,[1a] H. C. Silvis,[1a] T. A. Kent,[1b] B. H. Huynh,[1b] J. V. Waszczak,[1c] Boon-Keng Teo,*[1c] and B. A. Averill*[1a]

Contribution from the Department of Chemistry, Michigan State University, East Lansing, Michigan 48824, Gray Freshwater Biological Institute, University of Minnesota, Navarre, Minnesota 53392, and Bell Laboratories, Murray Hill, New Jersey 07974.
Received June 7, 1979

Abstract: The complex ions $[S_2MoS_2Fe(SR)_2]^{2-}$ (Ia, R = phenyl; Ib, R = *p*-tolyl) and $[S_2MoS_2FeCl_2]^{2-}$ (II) have been synthesized. Reaction of $(Et_4N)_2MoS_4$ with anhydrous $FeCl_2$ in acetonitrile affords the tetraethylammonium salt of II. The corresponding thiolate species Ia and Ib can be prepared from II by reaction with the corresponding thiol and Et_3N. The preparation and interconversion chemistry and the optical, ^1H NMR, and ^{57}Fe Mössbauer spectra of these compounds are described, as are the crystal structures of the Et_4N^+ salts of Ia and II. $(Et_4N)_2[FeMoS_4(SPh)_2]$ crystallizes in the monoclinic space group $P2_1/c$ with $Z = 4$ and unit cell parameters $a = 10.957$ (1) Å, $b = 10.794$ (1) Å, $c = 30.917$ (3) Å, $\beta = 97.37$ (1)°, and $V = 3626$ Å^3; the structure was refined to give $R_1 = 6.26\%$ and $R_2 = 8.78\%$, using 5531 independent reflections with $F_0 > 2\sigma(F_0)$. $(Et_4N)_2[FeMoS_4Cl_2]$ crystallizes in the monoclinic space group $P2_1/n$ with $Z = 2$ and unit cell parameters $a = 8.929$ (1) Å, $b = 10.215$ (1) Å, $c = 15.406$ (2) Å, $\beta = 103.40$ (1)°, and $V = 1367$ Å^3. The structure was refined to $R_1 = 5.48\%$ and $R_2 = 8.21\%$, using 2229 independent reflections with $F_0 > 2\sigma(F_0)$; the anions occupy an inversion center, resulting in a twofold disorder of the metal atoms (Mo, Fe) and the terminal atoms (S, Cl). The structures of both Ia and II consist of a dimetallic unit bridged by two sulfides, with two terminal sulfides on molybdenum and two phenyl mercaptides or chlorides on iron completing an essentially tetrahedral environment around each metal atom. The planar MoS_2Fe units in Ia and II, with Mo-Fe distances of 2.756 (1) and 2.786 (1) Å and Mo-S-Fe angles of 75.18 (6) and 76.00 (5)°, respectively, are very similar to the Fe_2S_2 units found in the $[Fe_2S_2(S\text{-}p\text{-}Tol)_4]^{2-}$ and $[Fe_2S_2Cl_4]^{2-}$ ions. Isotropically shifted resonances are observed in the ^1H NMR spectra of Ia and Ib; the directions and relative magnitudes of these shifts are consistent with significant delocalization of spin into the π system of the phenyl rings. The magnitude of the isotropic shifts *decreases* with increasing temperature, consistent with a simple paramagnetic system. Magnetic susceptibility measurements on Ia and II at 23 °C give values of $\mu_{eff} = 5.1$ and 5.3 μ_B, respectively, consistent with an $S = 2$ ground state. Zero field ^{57}Fe Mössbauer spectra of Ia and II in frozen *N,N*-dimethylformamide solution show a single quadrupole doublet. At 4.2 K the observed isomer shifts (0.47 and 0.60 mm/s, respectively) are between those observed for high-spin Fe^{2+} and Fe^{3+} in tetrahedral sulfur environments. Mössbauer spectra recorded at low temperatures and in high applied fields revealed that Ia has an easy axis of magnetization. The largest principal component of its electric field gradient is positive and approximately 12° from the easy axis. In addition, an anisotropic magnetic hyperfine interaction was observed which suggests a bonding scheme based on Fe(II) rather than Fe(III). The stability of the $[S_2MoS_2FeX_2]^{2-}$ unit, the short Mo-Fe distance, and the isomer shifts all suggest that the dimetallic unit is stabilized by an interaction involving net transfer of electron density from Fe(II) to Mo(VI).

Recent reports on the isolation[2] and physical properties[3,4] of a low molecular weight cofactor (the FeMo cofactor) from the MoFe protein of the enzyme nitrogenase suggest that it contains a novel Mo-Fe-S cluster. Extended X-ray absorption fine structure (EXAFS) results[5,6] indicate that the molybdenum atom has either three[6a] or two[5b,7] iron atoms and four or five sulfur atoms as nearest neighbors. Models consistent with these data include an Fe-S cubane-like cage with a molybdenum atom at one corner[6a] and an extended structure in which two Fe_4S_4 cubes are bridged by an S_2MoS_2 unit.[7] To date, only one related structural unit, consisting of two $MoFe_3S_4$ cubes linked through the Mo atoms via one sulfide and two mercaptide,[6a] three mercaptide,[6b,8] or $Fe(SR)_6$[6c] bridges, has been reported. Synthetic work on the related Fe-S clusters[9] suggests that a variety of structural types may be thermodynamically stable and accessible via self-assembly reactions of simple reagents. In particular, we are interested in preparing compounds containing MoS_2Fe or FeS_2MoS_2Fe units, in order to compare their properties with those of the $MoFe_3S_4$ cubane clusters as potential structural models for the FeMo cofactor of nitrogenase.

We have found that complexes of the general formula $[S_2MoS_2FeX_2]^{2-}$ (X = aromatic thiolate or halide) are readily formed by reaction of tetrathiomolybdate(VI) with monomeric Fe(II) starting materials or by degradation of a molybdenum-iron-sulfur compound containing coordinated tetrathiomolybdate. Such compounds are of particular interest in that acid hydrolysis of the MoFe protein of nitrogenase is reported to give high yields of thiomolybdates.[10] We describe herein the synthesis, optical, ^1H NMR, and ^{57}Fe Mössbauer spectra, and reactivity of several such compounds, and the X-ray structures of the $[S_2MoS_2Fe(SPh)_2]^{2-}$ and $[S_2MoS_2FeCl_2]^{2-}$ ions. Shortly before submission of this paper, Coucouvanis and co-workers[11a] reported an inde-

(1) (a) Michigan State University; (b) Gray Freshwater Biological Institute; (c) Bell Laboratories.
(2) V. K. Shah and W. J. Brill, *Proc. Natl. Acad. Sci. U.S.A.*, **74**, 3249 (1977).
(3) J. Rawlings, V. K. Shah, J. R. Chisnell, W. J. Brill, R. Zimmerman, E. Münck, and W. H. Orme-Johnson, *J. Biol. Chem.*, **253**, 1001 (1978).
(4) B. H. Huynh, E. Münck, and W. H. Orme-Johnson, *Biochim. Biophys. Acta*, **527**, 192 (1979).
(5) (a) S. P. Kramer, K. O. Hodgson, W. O. Gillum, and L. E. Mortenson, *J. Am. Chem. Soc.*, **100**, 3398 (1978); (b) S. P. Cramer, W. O. Gillum, K. O. Hodgson, L. E. Mortenson, E. I. Stiefel, J. R. Chisnell, W. J. Brill, and V. K. Shah, *ibid.*, **100**, 3814 (1978).
(6) (a) T. E. Wolff, J. M. Berg, C. Warrick, K. O. Hodgson, and R. H. Holm, *J. Am. Chem. Soc.*, **100**, 4630 (1978); (b) T. E. Wolff, J. M. Berg, K. O. Hodgson, R. B. Frankel, and R. H. Holm, *ibid.*, **101**, 4140 (1979); (c) T. E. Wolff, J. M. Berg, P. P. Power, K. O. Hodgson, R. H. Holm, and R. B. Frankel, *ibid.*, **101**, 5454 (1979).
(7) B.-K. Teo and B. A. Averill, *Biochem. Biophys. Res. Commun.*, **88**, 1454 (1979).
(8) (a) G. Christou, C. D. Garner, F. E. Mabbs, and T. J. King, *J. Chem. Soc., Chem. Commun.*, 740 (1978); (b) G. Christou, C. D. Garner, F. E. Mabbs, and M. G. B. Drew, *ibid.*, 91 (1979); (c) S. R. Acott, G. Christou, C. D. Garner, T. J. King, F. E. Mabbs, and R. M. Miller, *Inorg. Chim. Acta*, **35**, L337 (1979).
(9) R. H. Holm, *Acc. Chem. Res.*, **10**, 427 (1977).
(10) W. G. Zumft, *Eur. J. Biochem.*, **91**, 345 (1978).

0002-7863/80/1502-5550$01.00/0

pendent synthesis and X-ray structure determination of the $[S_2MoS_2Fe(SPh)_2]^{2-}$ ion. Very recently, the same group has reported the preparation and structures of the $[Cl_2FeS_2MoS_2FeCl_2]^{2-}$ [11b] and $[S_5FeS_2MS_2]^{2-}$ [11c] ions (M = Mo, W), while the preparation of a compound formulated as $(Et_4N)_3[(PhS)_2FeS_2FeS_2MoS_2]$ has been reported by Tieckelmann and Averill.[11d]

Experimental Section

Materials and Methods. All operations were performed in an atmosphere of dinitrogen or argon purified by passage over hot BASF catalyst R-3-11 and supported P_2O_5 (Aquasorb). Solvents and reagents were degassed by repeated evacuation and flushing with pure dinitrogen or argon before use. Acetonitrile and tetrahydrofuran were distilled from CaH_2 and Na/benzophenone, respectively. Mercaptans and *N,N*-dimethylacetamide (Gold Label) were obtained from Aldrich Chemical Co., Inc., and used without further purification. Triethylamine was stored over 4 Å molecular sieves. All other reagents were commercial reagent grade. Ammonium tetrathiomolybdate[12] and tetraalkylammonium salts of tetrathiomolybdate,[6b] $(Et_4N)_2[Fe_4S_4Cl_4]$,[13] $FeCl_2$,[14] and $(Et_4N)_3[Fe(MoS_4)_2]$[15] were prepared as described. Microanalyses were performed by Spang Microanalytical Laboratory, Eagle Harbor, Mich., and by Galbraith Laboratories, Inc., Knoxville, Tenn.

Physical Measurements. All samples were handled under anaerobic conditions. Optical spectra were obtained on either a Cary 219 or a Cary 17 spectrophotometer. ^1H NMR spectra were obtained on a Bruker WH-180 spectrometer. Magnetic susceptibility measurements at room temperature were performed on an Alpha Faraday balance; the variable temperature susceptibility data were obtained at Bell Laboratories on a Faraday-type apparatus previously described.[16] Melting points were obtained in sealed tubes in vacuo and are uncorrected. Electrochemical measurements were performed on a PAR 174A polarographic analyzer, using either dc polarography (dropping mercury electrode) or cyclic voltammetry (platinum electrode). Electron paramagnetic resonance (EPR) spectra were obtained on a Varian E-4 spectrometer operating at 9.1 GHz and equipped with an Oxford cryostat for operation from 4 to 300 K.

Mössbauer Methods. The Mössbauer spectrometer was of the constant acceleration type and has been described previously.[17] The 4.2 K measurements were performed with the sample immersed in liquid He. Room temperature Mössbauer spectra of a metallic Fe foil were used to calibrate the velocity scale and the centroid of these spectra was taken as zero velocity. Line widths in these calibration spectra were typically 0.25 mm/s. The frozen solution Mössbauer samples of Ia and II were prepared in an Ar atmosphere by dissolving the crystals in dimethylformamide (DMF) and then freezing the unsaturated solution. The samples were stored in liquid N_2 when not in use.

$(Et_4N)_2[FeMoS_4(SPh)_2]$. Method A. To 2.45 g of the compound formulated as $(Et_4N)_3[Fe(MoS_4)_2]$[15] (prepared from $(Et_4N)_2[Fe_4S_4(SEt)_4]$, 4 equiv of $(Et_4N)_2MoS_4$, and 4 equiv of 2,4,6-trimethylpyridinium hexafluorophosphate in acetonitrile) was added a solution of 37 mL of thiophenol and 50 mL of triethylamine (300 equiv of $Et_3NH^+PhS^-$) in 40 mL of acetonitrile. The initial red-violet solution changed to deep red-orange upon stirring for 1–2 h. The product was precipitated as dark red microcrystals by addition of 100 mL of tetrahydrofuran, collected by filtration, and washed with tetrahydrofuran.

Scheme I

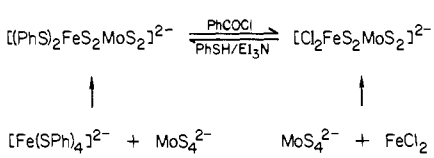

Recrystallization was effected by dissolution in a minimum amount of acetonitrile at room temperature, filtration, addition of 40 mL of tetrahydrofuran, and slow cooling to −20 °C. This afforded the product in ≥50% yield as 1-2-mm red-black prisms (mp 126–128 °C dec). Anal. Calcd for $C_{28}H_{50}FeMoN_2S_6$: C, 44.32; H, 6.64; Fe, 7.36; Mo, 12.64; N, 3.69; S, 25.35. Found: C, 44.20; H, 6.42; Fe, 7.55; Mo, 13.02; N, 3.86; S, 25.50.

Method B. To 0.20 g (0.33 mmol) of $(Et_4N)_2[FeMoS_4Cl_2]$ (see below) was added a solution of 0.13 mL of thiophenol and 0.18 mL of triethylamine (1.3 mmol of $Et_3NH^+PhS^-$) in 15 mL of acetonitrile. Reaction was virtually instantaneous, yielding the characteristic deep red-orange color. The product was precipitated in microcrystalline form by slow addition of 40 mL of tetrahydrofuran, collected, and recrystallized as above (yield ~45%).

$(Et_4N)_2[FeMoS_4(S\text{-}p\text{-}Tol)_2]$. This compound was prepared by method A above and obtained as red-black prisms (mp 131–134 °C dec) after recrystallization from acetonitrile. Anal. Calcd for $C_{30}H_{54}FeMoN_2S_6$: C, 45.78; H, 6.92; N, 3.56. Found: C, 45.77; H, 6.80; N, 3.58. Use of method B afforded the same compound together with an unidentified impurity that was difficult to remove by recrystallization.

$(Et_4N)_2[FeMoS_4Cl_2]$. To a slurry of 0.29 g (2.28 mmol) of anhydrous $FeCl_2$ in 10 mL of acetonitrile was added with vigorous stirring a solution of 1.0 g (2.06 mmol) of $(Et_4N)_2MoS_4$ in 100 mL of acetonitrile. After 10 h the solution was filtered and the filtrate reduced in vacuo to ~40 mL. Cooling to −20 °C gave the product as dark brown microcrystals; recrystallization from acetonitrile gave product as dark brown prisms (mp 217 °C dec) in ~80% yield. Anal. Calcd for $C_{16}H_{40}Cl_2FeMoN_2S_4$: C, 31.43; H, 6.59; Fe, 9.13; Mo, 15.69; N, 4.58. Found: C, 31.63; H, 7.00; Fe, 9.16; Mo, 15.77; N, 4.76. The same compound was also obtained in low yield from an acetonitrile solution containing 1 equiv of $(Et_4N)_2MoS_4$ and 2 equiv of $(Et_4N)_2[Fe_4S_4Cl_4]$ after brief exposure to the atmosphere and subsequent anaerobic workup.

Interconversion Reactions. A. $[FeMoS_4Cl_2]^{2-} \rightarrow [FeMoS_4(SPh)_2]^{2-}$. Treatment of a solution of 6.6 mg (11 μmol) of $(Et_4N)_2[FeMoS_4Cl_2]$ in 6.75 mL of acetonitrile with 3.3 μL (24 μmol) of triethylamine and 2.4 μL (24 μmol) of thiophenol resulted in an immediate color change from orange-brown to red-orange. The optical spectrum of the solution showed that $[FeMoS_4(SPh)_2]^{2-}$ was formed quantitatively.

B. $[FeMoS_4(SPh)_2]^{2-} \rightarrow [FeMoS_4Cl_2]^{2-}$. Treatment of a solution of 25 mg (0.33 μmol) of $(Et_4N)_2[FeMoS_4(SPh)_2]$ in 25 mL of acetonitrile with 9.0 μL (0.73 μmol) of benzoyl chloride resulted in an immediate color change from red-orange to orange-brown. The optical spectrum of the solution was consistent with quantitative formation of $[FeMoS_4Cl_2]^{2-}$.

Collection and Reduction of X-ray Data. The X-ray data for $(Et_4N)_2[S_2MoS_2Fe(SPh)_2]$ and $(Et_4N)_2[S_2MoS_2FeCl_2]$ were collected at Molecular Structure Corp., College Station, Texas. Tables IA and IB summarize the results of crystal data and details of the collection and reduction of X-ray diffraction data, respectively.

Solution and Refinement of the Structures. Solution and least-squares refinement of the structures were done at Bell Laboratories. The details are tabulated in Table IC. For the least-squares refinement of $(Et_4N)_2[S_2MoS_2FeCl_2]$, a point-by-point arithmetic-mean averaging scheme was applied to the scattering tables of M (viz., $f_M = (f_{Fe} + f_{Mo})/2$) and X (viz., $f_X = (f_S + f_{Cl})/2$). This procedure was necessary since the dianion $[S_2MoS_2FeCl_2]^{2-}$ is located at the crystallographic inversion center $\bar{1}$, such that there is a twofold disorder involving the $FeCl_2$ and the MoS_2 (terminal) moieties of the dianion. To test the correctness of this disorder model, full-matrix least-squares refinements were performed by using identical procedures, assuming that the dianion was $[Cl_2FeS_2FeCl_2]^{2-}$ or $[S_2MoS_2MoS_2]^{2-}$. The results are $R_1 = 8.40\%$ and $R_2 = 12.15\%$ for $[Cl_2FeS_2FeCl_2]^{2-}$ and $R_1 = 8.21\%$ and 13.40% for $[S_2MoS_2MoS_2]^{2-}$. Both of these R values are much worse than those obtained with the disorder model (cf. Table IC).

The final positional and thermal parameters, with errors estimated from the full variance-covariance matrix,[18e] are listed in Tables IIA and IIB for $(Et_4N)_2[S_2MoS_2Fe(SPh)_2]$ and $(Et_4N)_2[S_2MoS_2FeCl_2]$, respectively. Other details of the methods used for structure solution and refinement can be found in ref 18.

(11) (a) D. Coucouvanis, E. D. Simhon, D. Swenson, and N. C. Baenziger, *J. Chem. Soc., Chem. Commun.*, 361 (1979); (b) D. Coucouvanis, N. C. Baenziger, E. D. Simhon, P. Stremple, D. Swenson, A. Simopoulos, A. Kostikas, V. Petrouleas, and V. Papaefthymiou, *J. Am. Chem. Soc.*, **102**, 1732 (1980); (c) D. Coucouvanis, N. C. Baenziger, E. D. Simhon, P. Stremple, D. Swenson, A. Kostikas, A. Simopoulos, V. Petrouleas, and V. Papaefthymiou, *ibid.*, **102**, 1730 (1980); (d) R. H. Tieckelmann and B. A. Averill, *Inorg. Chim. Acta*, **46**, L35 (1980).

(12) G. Krüss, *Justus Liebigs Ann. Chem.*, **225**, 6 (1884).

(13) G. B. Wong, M. A. Bobrik, and R. H. Holm, *Inorg. Chem.*, **17**, 578 (1978).

(14) P. Kovacic and N. O. Brace, *Inorg. Synth.*, **6**, 172 (1960).

(15) H. C. Silvis, R. H. Tieckelmann, and B. A. Averill, *Inorg. Chim. Acta*, **36**, L423 (1979). The compound $(Me_4N)_6[Fe_4Mo_4S_{20}]$ has now been reformulated as $(Me_4N)_3[Fe(MoS_4)_2]$; the Et_4N^+ salt is prepared in an analogous fashion. Presumably the anion has a structure similar to that of the $[M(WS_4)_2]^{2-}$ ions, where M = Zn,[21a] Co.[21b] An independent synthesis of the $[Fe(MoS_4)_2]$ anion has recently been described (J. W. MacDonald, G. D. Friesen, and W. E. Newton, submitted for publication).

(16) F. J. DiSalvo, A. Menth, J. V. Waszczak, and J. Tauc, *Phys. Rev. B*, **6**, 4574 (1972).

(17) M. H. Emptage, R. Zimmermann, L. Que, Jr., E. Münck, W. D. Hamilton, and W. H. Orme-Johnson, *Biochim. Biophys. Acta*, **495**, 12 (1977).

Table I. Summary of Crystal Data, Collection and Reduction of X-ray Data, and Solution and Refinement of Structures (Et = C_2H_5, Ph = C_6H_5)

	$(Et_4N)_2[FeMoS_4(SPh)_2]$	$(Et_4N)_2[FeMoS_4Cl_2]$
A. Crystal Data		
crystal color	red-black	brown
crystal shape	prism	prism
crystal dimensions, mm^3	0.2 × 0.2 × 0.3	0.25 × 0.20 × 0.35
cell parameters (errors)		
a, Å	10.957 (1)	8.929 (1)
b, Å	10.794 (1)	10.215 (1)
c, Å	30.917 (3)	15.406 (2)
α, deg	90.	90
β, deg	97.37 (1)	103.40 (1)
γ, deg	90.	90
cell vol, $Å^3$	3626.3	1366.9
Z	4	2
Laue symmetry	monoclinic	monoclinic
space group	$P2_1/c$	$P2_1/n$
systematic absences	$h0l, l = 2n + 1$	$h0l, h + l = 2n + 1$
	$0k0, k = 2n + 1$	$0k0, k = 2n + 1$
equiv positions	$\pm(x, y, z)$	$\pm(x, y, z)$
	$\pm(x, {}^1/_2 - y, {}^1/_2 + z)$	$\pm({}^1/_2 + x, {}^1/_2 - y, {}^1/_2 + z)$
B. Collection and Reduction of X-ray Diffraction Data[18a]		
diffractometer	Enraf-Nonius CAD4	Enraf-Nonius CAD4
radiation (graphite monochromated)	Mo Kα	Mo Kα
temp, °C	23 ± 1	23 ± 1
crystal-to-detector distance, cm	21	21
counter aperture width, mm	2.0	2.0
incident-beam collimator diameter, mm	0.7	0.7
takeoff angle, deg	2.8	2.8
scan technique	θ-2θ	θ-2θ
scan rate (limits), deg/min	4-40	4-40
scan range, deg	1.0	1.0
background:scan time ratio	0.5	0.5
no./freq of std reflection	3/100	3/100
2θ limits, deg	0-54	0-54
cutoff of obsd data	$2\sigma(I)$	$2\sigma(I)$
unique data	8320	3151
p	0.05	0.05
C. Solution and Refinement[18b]		
technique of solution	heavy atom	
method of refinement	full-matrix least-squares[18c]	
isotropic convergence[18d]	$R_1 = 11.66\%$	$R_1 = 10.30\%$
	$R_2 = 13.35\%$	$R_2 = 13.07\%$
isotropic-anisotropic convergence	$R_1 = 6.26\%$	$R_1 = 5.48\%$
	$R_2 = 8.78\%$	$R_2 = 8.21\%$
max shifts (Δ/σ)	0.4(x, y, z), 1.4(x, C16)	1.4(x, y), 1.8(z)
	0.9(x, C28), 1.0(B)	2.6(B)
error of fit	1.81	1.93
data/parameter	5531/253	2229/118
anomalous dispersion cor		
$\Delta f'$ (real)	- 1.7 (Mo), 0.4 (Fe), 0.1 (S)	none
$\Delta f''$ (imag)	0.9 (Mo), 1.0 (Fe), 0.2 (S)	
max residual intensity of final diff map, $e/Å^3$	0.9 (mostly H's)	0.9 (mostly H's)

Results and Discussion

Synthesis and Interconversion Reactions. Reaction of equimolar amounts of tetrathiomolybdate(VI) with anhydrous ferrous chloride in acetonitrile results in formation of the $[S_2MoS_2FeCl_2]^{2-}$ ion, isolated in high yield as its tetraethylammonium salt. The corresponding aryl thiolate derivatives $[S_2MoS_2Fe(SAr)_2]^{2-}$ can be prepared in any of several ways: (i) by analogous reaction of a mononuclear source of Fe(II), e.g., $[Fe(SPh)_4]^{2-}$, with tetrathiomolybdate;[11a] (ii) by an exchange of aryl thiolate for halide on the preformed $[S_2MoS_2FeX_2]^{2-}$ core (this work); (iii) by degradation of the molybdenum–iron–sulfur species formulated as $[Fe(MoS_4)_2]^{3-}$, upon treatment with a large excess of aryl mercaptan and triethylamine. Route (i) clearly involves simple substitution of two thiophenolate ligands by a bidentate tetrathiomolybdate ligand. This mode of coordination is well established for tetrathiometalate ions of molybdenum and tungsten,[19-22]

(18) (a) The intensity I was calculated according to the expression $I = S(C - RB)$ where S is the scan rate, C is the total integrated peak count, R is the ratio of scan time to background counting time, and B is the total background count. The standard deviation of I was calculated as $\sigma(I) = [S^2(C + R^2B) + (pI)^2]^{1/2}$ where $p = 0.05$. The data were also corrected for Lorentz and polarization effects to yield the observed structure factor $|F_o| = [I/(Lp)]^{1/2}$ and its standard deviation $\sigma(F_o) = \sigma(I)/(2 \times |F_o| \times (Lp))$. No extinction or absorption correction was necessary. (b) Atomic scattering factors used for all nonhydrogen atoms are from H. P. Hanson, F. Herman, J. D. Lea, and S. Skillman, *Acta Crystallogr.*, **17**, 1040 (1964); those for the hydrogen atoms are from R. F. Stewart, E. R. Davidson, and W. T. Simpson, *J. Chem. Phys.*, **42**, 3175 (1965). (c) All least-squares refinements were based on the minimization of $\Sigma w_i||F_o| - |F_c||^2$ with the individual weights $w_i = 1/\sigma(F_o)^2$. (d) $R_1 = [\Sigma||F_o| - |F_c||/|F_o|] \times 100\%$ and $R_2 = [\Sigma w_i||F_o| - |F_c||^2/\Sigma w_i|F_o|^2]^{1/2} \times 100\%$. See supplementary material for a listing of observed and calculated structure factors. (e) ORFEE3 by W. R. Busing, K. O. Martin, and H. A. Levy with modifications by G. M. Brown, C. K. Johnson, and W. E. Thiessen, Oak Ridge National Laboratory, Oak Ridge, Tenn., 1971. (f) B.-K. Teo and P. A. Snyder-Robinson, *Inorg. Chem.*, **17**, 3489 (1978).

(19) E. Diemann and A. Müller, *Coord. Chem. Rev.*, **10**, 79 (1973).

(20) (a) A. Müller, E. Diemann, and H.-H. Heinsen, *Chem. Ber.*, **104**, 975 (1971); (b) A. Müller, E. Ahlborn, and H.-H. Heinsen, *Z. Anorg. Allg. Chem.*, **386**, 102 (1971); (c) A. Müller and S. Sarkar, *Angew. Chem., Int. Ed. Engl.*, **16**, 705 (1977).

Table II. Positional and Thermal Parameters with Esd's

A. $(Et_4N)_2[S_2MoS_2Fe(SPh)_2]$

atom	x	y	z	β, Å²
Mo	0.333 39 (5)	0.195 08 (5)	0.365 32 (2)	a
Fe	0.154 54 (8)	0.343 39 (8)	0.393 45 (3)	a
S1	0.3522 (1)	0.3935 (2)	0.3877 (1)	a
S2	0.1412 (2)	0.1394 (2)	0.3761 (1)	a
S3	0.3545 (2)	0.1838 (2)	0.2973 (1)	a
S4	0.4679 (2)	0.0824 (2)	0.4043 (1)	a
S5	0.0925 (2)	0.3868 (2)	0.4601 (1)	a
S6	0.0478 (1)	0.4808 (2)	0.3450 (1)	a
C1	0.1929 (5)	0.3229 (6)	0.5039 (2)	a
C2	0.2669 (6)	0.2213 (6)	0.4988 (2)	a
C3	0.6573 (7)	−0.1729 (7)	0.4648 (3)	a
C4	0.6584 (8)	−0.2262 (8)	0.4240 (2)	a
C5	0.7301 (8)	0.6681 (8)	0.4189 (2)	a
C6	0.1942 (7)	0.3786 (7)	0.5452 (2)	a
C7	−0.1120 (5)	0.4506 (6)	0.3384 (2)	a
C8	−0.1692 (6)	0.3821 (7)	0.3688 (2)	a
C9	0.7037 (6)	0.3622 (7)	0.3624 (2)	a
C10	0.6328 (7)	0.4112 (8)	0.3259 (3)	a
C11	0.6881 (7)	0.4794 (9)	0.2961 (3)	a
C12	0.1834 (6)	0.0025 (8)	0.1970 (3)	a

atom	β_{11}	β_{22}	β_{33}	β_{12}	β_{13}	β_{23}
Mo	54.7 (5)	57.1 (5)	7.3 (1)	2.1 (4)	2.2 (1)	0.2 (2)
Fe	52.3 (7)	67.7 (9)	7.9 (1)	0.3 (6)	2.7 (2)	0.7 (2)
S1	56.5 (14)	64.8 (15)	12.7 (2)	−9.0 (12)	5.6 (4)	−3.0 (5)
S2	65.3 (15)	69.9 (17)	13.4 (3)	−20.1 (13)	2.6 (5)	−2.6 (5)
S3	124.7 (22)	113.3 (22)	8.6 (2)	22.1 (18)	8.2 (5)	−2.1 (6)
S4	83.3 (17)	87.4 (19)	13.2 (3)	17.1 (15)	−1.4 (5)	6.8 (6)
S5	67.6 (15)	85.8 (17)	8.4 (2)	15.4 (13)	3.7 (4)	0.8 (5)
S6	55.5 (14)	104.6 (20)	11.1 (2)	−3.9 (14)	2.5 (5)	12.2 (5)
C1	62 (5)	71 (6)	8 (1)	−13 (5)	4 (2)	4 (2)
C2	73 (6)	70 (7)	12 (1)	−3 (5)	4 (2)	1 (2)
C3	103 (8)	98 (8)	13 (1)	10 (6)	−2 (2)	5 (2)
C4	122 (9)	121 (10)	10 (1)	3 (8)	1 (2)	7 (2)
C5	125 (9)	130 (10)	9 (1)	8 (8)	3 (2)	3 (2)
C6	98 (7)	95 (8)	9 (1)	−6 (6)	7 (2)	0 (2)
C7	54 (5)	76 (7)	9 (1)	7 (5)	3 (2)	−1 (2)
C8	74 (6)	90 (7)	10 (1)	−12 (5)	6 (2)	3 (2)
C9	76 (7)	108 (8)	10 (1)	−4 (6)	0 (2)	3 (2)
C10	73 (7)	139 (10)	17 (1)	3 (7)	2 (2)	14 (3)
C11	78 (7)	197 (13)	16 (1)	−17 (8)	−6 (2)	28 (3)
C12	73 (7)	149 (10)	13 (1)	0 (7)	−2 (2)	−19 (3)

B. $(Et_4N)_2[S_2MoS_2FeCl_2]$

atom	x	y	z	β, Å²
M	0.056 20 (7)	0.411 21 (6)	0.446 65 (4)	a
S1	0.1470 (2)	0.6137 (1)	0.4907 (1)	a
X2	0.0151 (2)	0.6040 (2)	0.6995 (1)	a
X3	0.2334 (2)	0.2626 (2)	0.4971 (1)	a

atom	β_{11}	β_{22}	β_{33}	β_{12}	β_{13}	β_{23}
M	134.3 (10)	80.6 (7)	48.3 (4)	−8.4 (6)	28.1 (4)	−0.5 (4)
S1	144.8 (23)	77.6 (15)	59.0 (9)	−22.1 (14)	39.3 (12)	4.6 (9)
X2	188.6 (30)	181.2 (28)	46.7 (8)	−15.1 (22)	26.5 (13)	−6.6 (12)
X3	169.3 (28)	89.8 (17)	83.2 (12)	8.6 (18)	24.6 (14)	1.9 (11)

[a] Anisotropic thermal parameters (×10⁴) of the form $\exp[-(h^2\beta_{11} + k^2\beta_{22} + l^2\beta_{33} + 2hk\beta_{12} + 2hl\beta_{13} + 2kl\beta_{23})]$ are given in the second part of this table.

although the present complexes are the first examples of a stoichiometry other than $[M(S_2M'S_2)_2]^{2-}$.

Formation of $[S_2MoS_2Fe(SAr)_2]^{2-}$ from $[S_2MoS_2FeCl_2]^{2-}$ occurs rapidly and essentially quantitatively upon addition of 2–3 equiv of aryl mercaptan and triethylamine, demonstrating that substitution of the terminal ligands on iron is facile. Similarly, addition of 2 equiv of benzoyl chloride to the aryl thiol derivative Ia results in immediate and quantitative formation of the chloro species II, as shown by the appearance and disappearance of the characteristic optical spectra (Figure 3). Excess benzoyl chloride causes slow decomposition with the formation of a black solid. These reactions are entirely analogous to those observed for the Fe_2S_2 and Fe_4S_4 clusters,[13,23] and establish that the iron portion of the binuclear MoFe unit possesses reactivity comparable to that of the diiron analogue.[13] The S_2MoS_2Fe unit reacts only very slowly with ca. 300–400 equiv of thiophenoxide, suggesting that tetrathiomolybdate has a high affinity for iron. The reactions are summarized in Scheme I.

Description of the Structures. The crystal structures of $(Et_4N)_2[S_2MoS_2Fe(SPh)_2]$ and $(Et_4N)_2[S_2MoS_2FeCl_2]$ consist of discrete cations and anions in an 8:4 and a 4:2 ratio per unit cell. Crystallographically, there are two independent cations and one independent dianion per asymmetric unit for $(Et_4N)_2$-

(21) (a) I. Paulat-Böschen, B. Krebs, A. Müller, E. Königer-Ahlborn, H. Dornfeld, and H. Schultz, *Inorg. Chem.*, **17**, 1440 (1978); (b) A. Müller, N. Mohan, and H. Bögge, *Z. Naturforsch. B*, **33**, 978 (1978).

(22) I. Sotofte, *Acta Chem. Scand., Ser. A*, **30**, 157 (1976).

(23) R. W. Johnson and R. H. Holm, *J. Am. Chem. Soc.*, **100**, 5338 (1978).

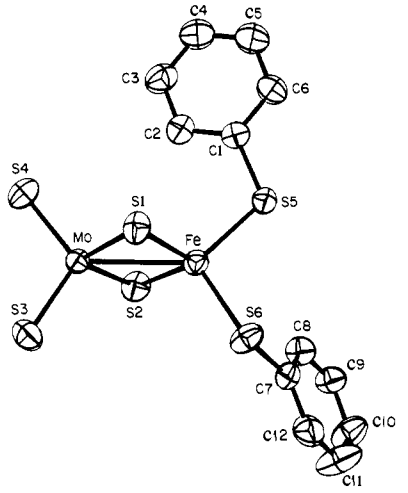

Figure 1. Stereochemistry of the $[S_2MoS_2Fe(SPh)_2]^{2-}$ dianion. Hydrogen atoms are omitted for clarity.

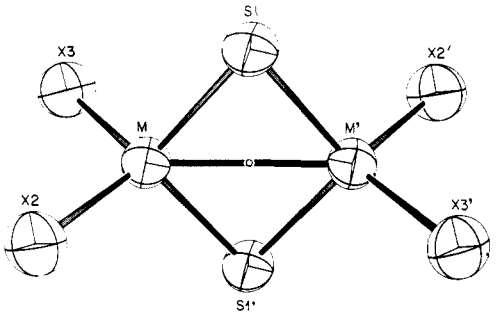

Figure 2. Stereochemistry of the $[S_2MoS_2FeCl_2]^{2-}$ dianion. The crystallographic C_i-$\bar{1}$ site symmetry causes a twofold disorder of the metal atoms (M = (Mo + Fe)/2) and the terminal ligands (X = (S + Cl)/2).

$[S_2MoS_2Fe(SPh)_2]$, but one independent cation and one-half of the dianion for $(Et_4N)_4[S_2MoS_2FeCl_2]$. Since the dianion $[S_2MoS_2FeCl_2]^{2-}$ in the latter structure is located at the crystallographic inversion center ($\bar{1}$), there is a twofold disorder involving the $FeCl_2$ and the MoS_2 (terminal) moieties of the dianion. In this structure, the crystallographically independent metal atom (M) and the two independent terminal ligands (X_2 and X_3) were successfully refined as equal admixtures of Fe and Mo and Cl and S, respectively (vide supra).

The structures of the dianions, $[S_2MoS_2Fe(SPh)_2]^{2-}$ (Ia) and $[S_2MoS_2FeCl_2]^{2-}$ (II), are portrayed in Figures 1 and 2, respectively, while the pertinent molecular parameters are listed in Tables III and IV. The structures can be described as containing two tetrahedral units, MoS_4 and S_2FeX_2, where X = SPh for Ia and Cl for II, joined at a common edge. The six bond angles around each of the metal atoms are all very close to the ideal tetrahedral value of 109.49° (range 104–117° for Ia and 104–112° for II). The Mo–Fe distances in the dianions $[S_2MoS_2Fe(SPh)_2]^{2-}$ and $[S_2MoS_2FeCl_2]^{2-}$ are 2.756 (1) and 2.786 (1) Å, respectively. While these values approach a single covalent bond value and thus may indicate significant interaction between the two metal atoms, the detailed nature of the electronic structure of these dianions remains unsettled.

Comparison of the mixed bimetallic cores of Ia and II reveals several structural trends. In Ia, the terminal Mo–S bonds (2.153 (2) Å) are substantially shorter than the bridging Mo–S bonds (2.225 (2) Å). The latter are similar to the bridging Fe–S bonds (2.264 (2) Å), which are in turn significantly shorter than the terminal Fe–S(Ph) bonds (2.307 (2) Å). In II, the crystal disorder of Mo and Fe as well as the terminal sulfurs and chlorides results in the average bridging metal–sulfur bonds of 2.263 (2) Å and terminal metal–ligand bonds of 2.200 (2) Å. These values are close to the corresponding values or averages in Ia.

Comparison of the Mo–Fe–S clusters Ia and II with the corresponding Fe–S dimers, $[(p\text{-TolS})_2FeS_2Fe(S\text{-}p\text{-Tol})_2]^{2-}$ (III) and

Table III. Interatomic Distances (Å) with Esd's

	A. $(Et_4N)_2[S_2MoS_2Fe(SPh)_2]$		
	1. The Dianion		
core		phenyls	
Mo-Fe	2.756 (1)	C1-C2	1.385 (9)
Mo-S1	2.253 (2)	C2-C3	1.410 (10)
Mo-S2	2.256 (2)	C3-C4	1.390 (11)
Mo-S3	2.149 (2)	C4-C5	1.405 (11)
Mo-S4	2.157 (2)	C5-C6	1.392 (10)
Fe-S1	2.262 (2)	C6-C1	1.409 (9)
Fe-S2	2.267 (2)	C7-C8	1.404 (9)
Fe-S5	2.299 (2)	C8-C9	1.398 (9)
Fe-S6	2.315 (2)	C9-C10	1.391 (10)
S5-C1	1.772 (6)	C10-C11	1.378 (11)
S6-C7	1.766 (6)	C11-C12	1.418 (10)
		C12-C7	1.380 (9)
	2. Nonbonded Distances		
S1···S2	3.576 (2)	S1···S5	3.840 (2)
S1···S3	3.600 (3)	S1···S6	3.553 (2)
S1···S4	3.603 (3)	S2···S5	3.809 (3)
S2···S3	3.619 (3)	S2···S6	3.911 (3)
S2···S4	3.627 (3)	S5···S6	3.672 (3)
S3···S4	3.556 (3)		
	B. $(Et_4N)_2[S_2MoS_2FeCl_2]$		
	1. The Dianion		
M-M'	2.786 (1)	M-X2	2.199 (2)
M-S1	2.268 (2)	M-X3	2.200 (2)
M-S1'	2.258 (2)		
	2. Nonbonded Distances		
S1···S1'	3.566 (3)	S1'···X2	3.674 (2)
S1···X2	3.696 (3)	S1'···X3	3.669 (2)
S1···X3	3.665 (2)	X2···X3	3.583 (3)

Table IV. Bond Angles (deg) with Esd's

	A. $(Et_4N)_2[S_2MoS_2Fe(SPh)_2]$		
core		phenyls	
Mo-S1-Fe	75.26 (6)	S5-C1-C2	122.4 (5)
Mo-S2-Fe	75.10 (6)	S5-C1-C6	117.4 (5)
S1-Mo-S2	104.97 (6)	S6-C7-C8	122.8 (5)
S1-Mo-S3	109.72 (8)	S6-C7-C12	118.0 (5)
S1-Mo-S4	109.60 (8)	C1-C2-C3	119.7 (7)
S2-Mo-S3	110.45 (8)	C2-C3-C4	119.9 (7)
S2-Mo-S4	110.56 (8)	C3-C4-C5	120.5 (7)
S3-Mo-S4	111.34 (8)	C4-C5-C6	119.4 (7)
S1-Fe-S2	104.33 (7)	C5-C6-C1	120.2 (7)
S1-Fe-S5	114.70 (7)	C6-C1-C2	120.2 (6)
S1-Fe-S6	101.85 (7)	C7-C8-C9	120.6 (6)
S2-Fe-S5	113.09 (7)	C8-C9-C10	119.9 (7)
S2-Fe-S6	117.21 (8)	C9-C10-C11	119.9 (7)
S5-Fe-S6	105.44 (7)	C10-C11-C12	120.3 (7)
Fe-S5-C1	112.36 (22)	C11-C12-C7	120.0 (7)
Fe-S6-C7	111.56 (22)	C12-C7-C8	119.1 (6)
	B. $(Et_4N)_2[S_2MoS_2FeCl_2]$		
M-S1-M'	76.00 (5)	S1'-M-X2	111.04 (7)
S1-M-S1'	104.00 (5)	S1'-M-X3	110.77 (7)
S1-M-X2	111.69 (7)	X2-M-X3	109.06 (8)
S1-M-X3	110.24 (7)		

Table V. Selected Average Molecular Parameters (Distances in Angstroms and Angles in Degrees) for the Dianionic Bimetallic Clusters $[S_2MoS_2{*}FeX_2]^{2-}$ where X = SPh (Ia), Cl (II) and $[X_2FeS_2{*}FeX_2]^{2-}$ where X = S-*p*-Tol (III), Cl (IV)

parameter	Ia	II	III	IV
M-Fe[a]	2.756 (1)	2.786 (1)	2.691 (1)	2.716 (1)
Mo-S*	2.255 (2)	2.263 (2)		
Fe-S*	2.264 (2)		2.201 (1)	2.201 (1)
Mo-S	2.153 (2)	2.200 (2)		
Fe-X	2.307 (2)		2.312 (1)	2.252 (1)
S*···S*'	3.576 (2)	3.566 (3)	3.483 (3)	3.463
M-S*-Fe[a]	75.18 (6)	76.00 (5)	75.39 (4)	76.21 (3)
S*-Mo-S*'	104.97 (6)	104.00 (5)	104.61 (4)	103.79 (3)
S*-Fe-S*'	104.33 (7)			
S-Mo-S	111.34 (8)	109.06 (8)	111.2	105.37 (4)
X-Fe-X'	105.44 (7)			

[a] M = Mo for Ia and II and Fe for III and IV.

Table VI. Electronic Spectral Features, Magnetic Moments, and Isotropic Shifts of Mercaptide Protons of $[S_2MoS_2FeX_2]^{2-}$ Complexes

	$[S_2MoS_2Fe(SPh)_2]^{2-}$	$[S_2MoS_2Fe(S\text{-}p\text{-}Tol)_2]^{2-}$	$[S_2MoS_2FeCl_2]^{2-}$
electronic spectral features[a]	930 (1.1), 610 (sh), 550 (sh), 489 (101), 419 (91), 332 (171), 300 (183), 267 (273)	552 (sh), 491 (97), 418 (84), 332 (159), 301 (176), 265 (268)	1080 (1.2), 594 (sh), 528 (sh), 469 (64), 432 (48), 314 (124), 290 (110)
magnetic moment,[b] μ_B	5.1	c	5.3
isotropic shifts of mercaptide protons,[d] ppm	~14.6 (*o*-H), −29.2 (*m*-H), 43.7 (*p*-H)[e]	−31.0 (*m*-H), −47.8 (*p*-CH_3)[f]	

[a] In acetonitrile solution, except for low intensity features at $\lambda > 800$ nm, which were measured in concentrated dimethyl sulfoxide solution; 23 °C. λ_{max} (ϵ) in nm (M^{-1} cm^{-1} × 10^{-2}). [b] In the solid state at 23 °C. [c] Not determined. [d] In CD_3CN solution, shifts vs. diamagnetic mercaptans. Chemical shifts downfield of Me_4Si are taken as negative. [e] 20 °C. [f] 25 °C.

$[Cl_2FeS_2FeCl_2]^{2-}$ (IV), reveals significant stereochemical similarities (cf. Table V). Nevertheless, there are certain well-defined structural trends that deserve some comments. First, substitution of the mercaptides (SR) in Ia or III by the chlorides in II or IV, respectively, causes a slight increase in the metal–metal distance (ca. 0.03 Å). Substitution of one of the iron atoms in III or IV by a molybdenum atom in Ia or II, respectively, also causes a significant increase in the metal–metal distance (ca. 0.07 Å). The latter trend may be correlated with the larger covalent radius of molybdenum (1.30 Å for Mo vs. 1.17 Å for Fe). Second, the Mo–S* (where the asterisk denotes the bridging sulfurs) and Fe–S* distances in Ia are very similar (2.255 (2) and 2.264 (2) Å, respectively), despite the difference in the covalent radii of the two metals. These values are also virtually identical with the average of 2.263 (2) Å observed in II. The metal–sulfur (bridging) distances in Ia and II are, however, substantially longer (by ca. 0.06 Å) than the Fe–S* distances of 2.201 (1) Å found in III and IV. Third, the metal–(terminal ligand) distances appear to be less affected by the formal replacement of the iron atom by the molybdenum atom. Terminal Mo–S, Fe–S, and Fe–Cl distances average about 2.15, 2.31, and 2.25 Å, respectively, for Ia, III, and IV, which are crystallographically ordered. In particular, Fe–S (mercaptide) distances in Ia and III are virtually identical. Using the above values, we predict the M–X distance in II, which exhibits twofold disorder, to be 2.20 Å. The observed average is 2.200 (2) Å. Fourth, the average bridging metal–sulfur–metal angle in Ia–IV is highly acute and remains virtually constant (ca. 76°) throughout the series.

All the tetraethylammonium cations are crystallographically ordered with normal bond lengths and angles. Positional and thermal parameters, interatomic distances, and bond angles are given in the supplementary material (Tables VIII–X).

Electronic Spectra. The electronic absorption spectra of the $[S_2MoS_2Fe(SPh)_2]^{2-}$ and $[S_2MoS_2FeCl_2]^{2-}$ ions are shown in Figure 3; peak positions and extinction coefficients are presented in Table VI. The spectra of both the aryl thiolate and chloro complexes are dominated by a pair of intense absorptions between 400 and 500 nm. They are thus at least superficially similar to those reported for bis(tetrathiometalate) complexes of first-row transition metals, where a roughly symmetrical splitting of the lowest energy S → M charge-transfer transition of the parent tetrathiometalate is observed.[19,20a] Inasmuch as relatively low energy sulfide, mercaptide, or chloride to iron charge transfer transitions may also be expected[13,24,25] and the spectra clearly contain additional features in excess of those attributable to localized tetrathiometalate transitions, definitive assignment must await detailed calculations.

Oxidation–Reduction Properties. Polarographic and cyclic voltammetric studies on ca. 1 mM solutions of Ia and II in *N*,*N*-dimethylacetamide (DMA) with 50 mM $[Et_4N][ClO_4]$ supporting electrolyte over the range +1.0 to −2.0 V showed evidence for only a single electrochemically irreversible reduction at −1.34 and −1.33 V vs. SCE, respectively. The slopes of plots of log $[i/(i_d - i)]$ vs. voltage (diffusion currents, μA/mM FeMo) were 85 (1.4) and 108 mV (1.8), respectively. These results are in contrast to those obtained for the $[Fe_2S_2(SR)_4]^{2-}$ ions,[25] where two electrochemically reversible one-electron reductions are observed, but are similar to the observed irreversible reductions of $[Fe_2S_2X_4]^{2-}$ (X = halide).[13]

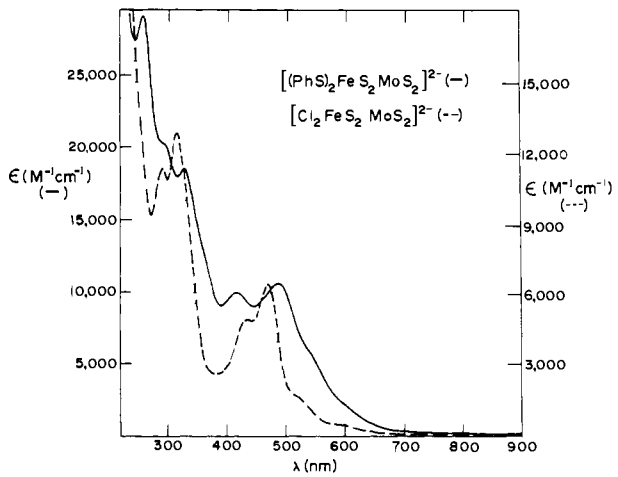

Figure 3. Electronic spectra of $(Et_4N)_2[S_2MoS_2Fe(SPh)_2]$ and $(Et_4N)_2[S_2MoS_2FeCl_2]$ in acetonitrile solution at 20 °C.

In view of possible problems associated with adsorption of these sulfur-rich complexes to metal electrode surfaces, attempts at generating a trianion by chemical means were made. Addition of 1–3 equiv of sodium acenaphthalenide radical anion ($ACN^{-\cdot}$) in THF to DMA solutions of Ia, followed by freezing and examination by EPR spectroscopy, gave no evidence for formation of a stable half-integral spin species. Instead, only the disappearance of the broad, weak absorption at $g \sim 8.6$ observed for Ia at 4–20 K (tentatively ascribed to a transition of the $S = 2$ spin system) was observed at a ratio of $ACN^{-\cdot}$: Ia of 1:1, together with the disappearance of the $g = 2$ signal of the radical anion. Thus, at this point we have no evidence for the stability of the one-electron reduced species $[S_2MoS_2FeX_2]^{3-}$, which would formally contain Fe(II) and Mo(V).

Magnetic Susceptibility. The magnetic susceptibility of $(Et_4N)_2[S_2MoS_2Fe(SPh)_2]$ and $(Et_4N)_2[S_2MoS_2FeCl_2]$, measured on solid samples at room temperature, corresponds to effective magnetic moments of 5.1 and 5.3 μ_B, respectively, per formula unit. This is consistent with the presence of four unpaired electrons ($S = 2$). The observed values fall well within the range (4.9–5.5 μ_B) reported for simple, monomeric high-spin Fe(II) complexes,[26] but are also consistent with an intramolecular antiferromagnetic Fe(III) (high-spin d^5)–Mo(V) (d^1) interaction.

The magnetic susceptibility of polycrystalline $(Et_4N)_2[S_2MoS_2Fe(SPh)_2]$ was measured from 4.2 to 300 K, using the Faraday method. At 300 K the magnetic susceptibility is independent of the applied field from 1.28 to 0.26 T, indicating that no ferromagnetic impurities were present in the sample. A temperature-dependent susceptibility is observed (Figure 4). From 300 to 30 K the susceptibility can be fitted with the Curie–Weiss

(24) B. V. DePamphilis, B. A. Averill, T. Herskovitz, L. Que, Jr., and R. H. Holm, *J. Am. Chem. Soc.*, **96**, 4159 (1974).
(25) J. J. Mayerle, S. E. Denmark, B. V. DePamphilis, J. A. Ibers, and R. H. Holm, *J. Am. Chem. Soc.*, **97**, 1032 (1975).
(26) B. N. Figgis and J. Lewis, *Prog. Inorg. Chem.*, **6**, 37 (1964).

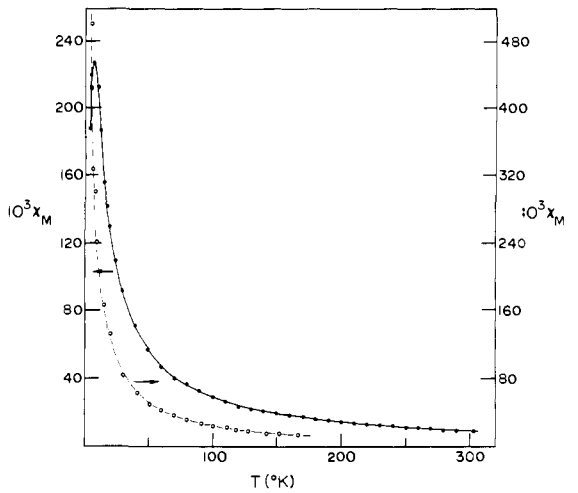

Figure 4. Magnetic susceptibility of $(Et_4N)_2[S_2MoS_2Fe(SPh)_2]$ as a function of temperature in the solid state (●) and in *N,N*-dimethylformamide glass (○), obtained in 0.16-T applied field. The left vertical axis refers to the solid, and the right to the frozen solution data. The solid and dashed lines are fits to the data as described in the text.

formula $\chi = C/(T + \theta) + \chi_0$. A least-squares fit to this equation gives on a per mole basis $\theta = 4.2$ K, $C_m = 3.187$ (emu·K)/mol, and $\chi_0 = -5.96 \times 10^{-4}$ emu/mol. From the Curie constant, the effective moment is calculated to be 5.05 μ_B/formula unit. Below 30 K the susceptibility shows a maximum near 8 K indicating antiferromagnetic coupling. Such antiferromagnetic coupling is consistent with the positive θ value obtained from the fit to the susceptibility above 30 K.

In order to distinguish between inter- and intramolecular antiferromagnetic couplings, a second sample in which the compound was dissolved in *N,N*-dimethylformamide (DMF) and frozen to yield a glass matrix was prepared. Such dilution will decrease the strength of intermolecular interactions, but should not affect intramolecular interactions. The glassy sample also showed a temperature-dependent susceptibility. However, no antiferromagnetic ordering was observed above 4.2 K, and the θ value for this sample decreased to 1.2 K. The fact that no antiferromagnetic ordering was observed in the frozen solution sample suggests that in the crystalline form intermolecular interactions exist and the magnetic order below 8 K is a long-range ordering. Mössbauer data at 4.2 K (see below) also support this interpretation. Detailed magnetic studies, including heat capacity and magnetic anisotropy measurements, are in progress and will be reported elsewhere. The results presented above, together with the negative temperature coefficient observed for isotropic shifts of mercaptide protons of Ia and Ib (see below), indicate that, if an antiferromagnetically coupled Fe(II)–Mo(V) formulation is correct, then $|2J| \gg kT$ even at 370 K.

Proton Magnetic Resonance Spectra. Proton magnetic resonance spectra have been obtained for the mercaptide complexes Ia and Ib as a function of temperature in polar organic solvents. In addition to the expected resonances of the cation, isotropically shifted resonances due to mercaptide protons are observed. The ^{1}H NMR spectra of Ia and Ib are shown in Figure 5, while the temperature dependence of the isotropic shifts is shown in Figure 6. Isotropic shifts of the mercaptide protons are summarized in Table VI.

In the phenyl derivative, the meta protons are shifted to low field and the ortho and para protons to high field (upfield of Me_4Si). Assignments are based on the relative line widths and on substitution of the *p*-H by CH_3. The broad resonance at ~+7 ppm in both the phenyl and *p*-tolyl derivatives is clearly attributable to the proton in the ortho position, as dipolar broadening is expected to have a $1/r^6$ dependence.[27] Replacement of the *p*-H

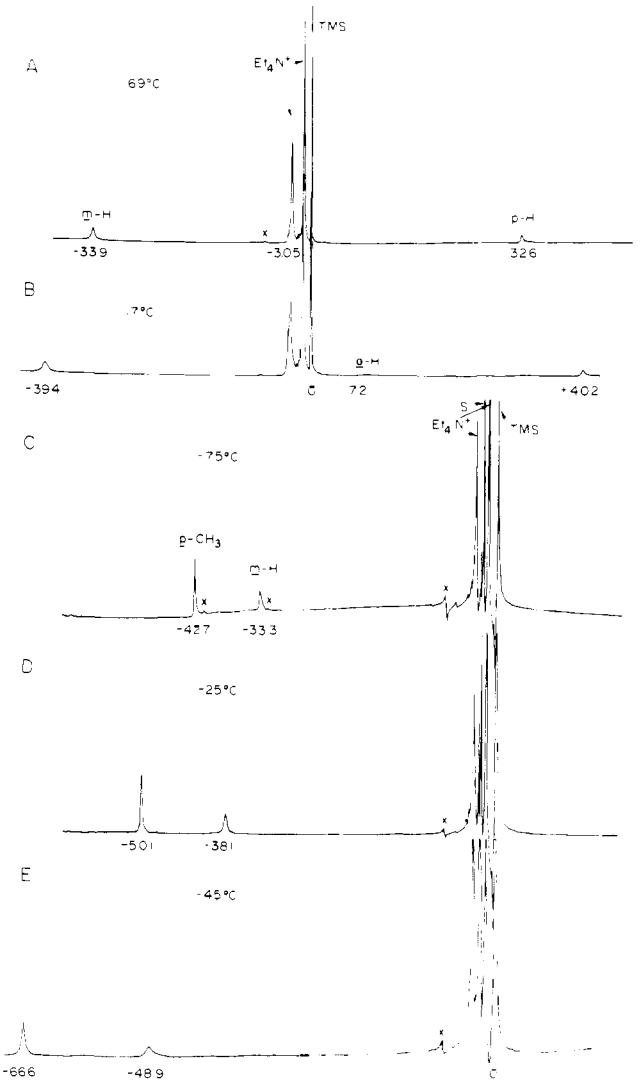

Figure 5. (A, B) ^{1}H NMR spectra (180 MHz) of $(Et_4N)_2[S_2MoS_2Fe(SPh)_2]$ in Me_2SO-d_6 at 69 and 17 °C. (C–E) ^{1}H NMR spectra of $(Et_4N)_2[S_2MoS_2Fe(S$-*p*-$Tol)_2]$ in CD_3CN at −45, 25, and 75 °C. Residual solvent proton resonances are indicated by S; impurities present in small amounts are denoted by X. Chemical shifts are in parts per million from Me_4Si.

by CH_3 results in the disappearance of the peak at +40 ppm and the appearance of a new resonance at ~−35 ppm with intensity corresponding to three protons. The results are thus qualitatively similar to those observed with aromatic thiolate derivatives of the Fe_4S_4 clusters,[28] and suggest that a dominant contact interaction is responsible for the observed isotropic shifts at the meta and para positions. The magnitude of the isotropic shifts observed for the *o*-H's, however, is less than that observed for the *m*-H's (ratio = −0.47 for the phenyl compound, −0.40 for the *p*-tolyl compound), suggesting that either the molecular orbital containing unpaired spin density has substantially different character from the normal HOMO[28-31] or that a dipolar contribution of opposite sign to the contact contribution is present. The appreciable magnetic anisotropy expected for the system and the r^{-3} dependence of the dipolar term[27] could make the latter effect important for the *o*-H's, and explain the observed data. Completion of the magnetic an-

(27) W. D. Horrocks, Jr., in "NMR of Paramagnetic Molecules: Principles and Applications", G. N. LaMar, W. D. Horrocks, Jr., and R. H. Holm, Eds., Academic Press, New York, 1973, Chapter 4.

(28) R. H. Holm, W. D. Phillips, B. A. Averill, J. Mayerle, and T. Herskovitz, *J. Am. Chem. Soc.*, **96**, 2109 (1974).

(29) (a) D. R. Eaton, A. D. Josey, W. D. Phillips, and R. E. Benson, *J. Chem. Phys.*, **37**, 347 (1962); (b) D. R. Eaton, A. D. Josey, and R. E. Benson, *J. Am. Chem. Soc.*, **89**, 4040 (1967).

(30) A. Carrington and I. C. P. Smith, *Mol. Phys.*, 9, 137 (1965).

(31) (a) T. J. Stone and W. A. Waters, *Proc. Chem. Soc., London*, 253 (1962); (b) A. Hudson and K. D. J. Root, *J. Chem. Soc. B*, 656 (1970).

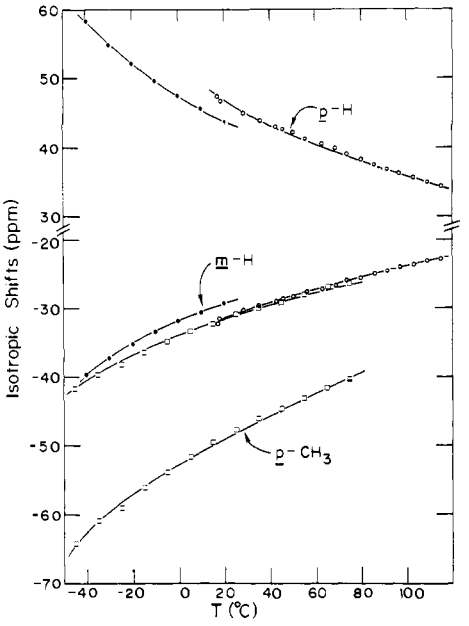

Figure 6. Temperature dependence of *m*-H, *p*-H, and *p*-CH_3 resonances of $(Et_4N)_2[S_2MoS_2Fe(SPh)_2]$ in Me_2SO-d_6 (○) and CD_3CN (●), and of $(Et_4N)_2[S_2MoS_2Fe(S\text{-}p\text{-}Tol)_2]$ in CD_3CN (□) solutions.

isotropy studies discussed above will permit us to examine this alternative in more detail.

The observed isotropically shifted mercaptide resonances are highly temperature dependent, with the magnitude of the shifts decreasing with increasing temperature. Data for the *m*- and *p*-H and the *p*-CH_3 protons of the phenyl and *p*-tolyl complexes are plotted in Figure 6; the resonances of the *o*-H's were so broad that precise peak positions could not be reliably measured. The temperature dependence of the observed shifts parallels that of the magnetic susceptibility, giving approximate Curie law behavior.[32]

Mössbauer Results. The susceptibility data have shown Ia to be paramagnetic with net electronic spin $S = 2$. Mössbauer spectroscopy provides additional data pertaining to the distribution of the unpaired spins about the iron nucleus. Mössbauer spectra of polycrystalline and frozen solution samples of Ia were recorded in magnetic fields from 0 to 6 T applied parallel to the γ beam and at temperatures from 1.5 to 160 K. At 4.2 K and in zero applied field the polycrystalline sample exhibited a well-defined magnetic spectrum with an overall splitting of 7.5 mm/s. An identical spectrum was observed with a 0.06 T field applied either parallel or perpendicular to the γ beam. Together these spectra indicate an ordering of the electron moments within the crystal. At 35 K the spectrum collapsed into a slightly broadened doublet with quadrupole splitting $\Delta E_Q = 1.73$ mm/s and isomer shift $\delta = 0.47$ mm/s. The frozen DMF solution sample was magnetically dilute and, compared with the polycrystalline form, offers more information about the local iron environment and is more readily compared with biological complexes. Therefore, we chose to concentrate on this form.

Spectra of the solution sample of Ia were interpreted by using the $S' = 2$ spin Hamiltonian given below.

$$\mathcal{H} = D[S_z'^2 - 2 + (E/D)(S_x'^2 - S_y'^2)] + 2\beta_e H^{app}\cdot S' + g_n^1\beta_n I\cdot\mathbf{A}\cdot S' - g_n^1\beta_n H^{app}\cdot I + \mathcal{H}_{Q^1} \quad (1)$$

The first term describes the zero-field splitting of the quintet and the second is the electronic Zeeman interaction where H^{app} is the applied field and $g = 2$. The third term is the magnetic hyperfine interaction between the electronic and ^{57}Fe nuclear spins. The fourth accounts for the direct interaction of the applied field and the nuclear moment. $\mathcal{H}_{Q^{3/2}}$ is the interaction of the electric quadrupole moment of the excited ^{57}Fe nucleus ($I = {}^3/_2$) with the electric field gradient (efg) produced at the nucleus by surrounding

(32) J. P. Jesson in ref 27, Chapter 1.

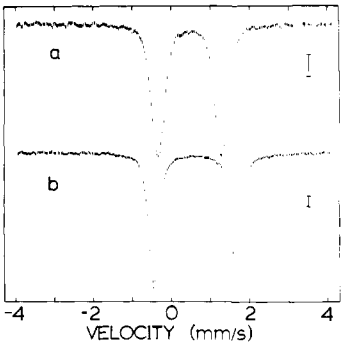

Figure 7. Mössbauer spectra of frozen DMF solutions of (a) $(Et_4N)_2[S_2MoS_2Fe(SPh)_2]$ and (b) $(Et_4N)_2[S_2MoS_2FeCl_2]$ recorded at 4.2 K and with zero applied field. Vertical bars indicate 1% absorption.

charges. In the frame in which the efg tensor is diagonal we may write $\mathcal{H}_{Q^{3/2}}$ as

$$\mathcal{H}_{Q^{3/2}} = eQ\frac{V_{\hat{z}\hat{z}}}{4}\left[I_{\hat{z}}^2 - \frac{5}{4} + \frac{\eta}{3}(I_{\hat{x}}^2 - I_{\hat{y}}^2) \right] \quad (2)$$

$$\eta = (V_{\hat{x}\hat{x}} - V_{\hat{y}\hat{y}})/V_{\hat{z}\hat{z}}$$

where Q is the ^{57}Fe nuclear quadrupole moment; $\hat{x}$, $\hat{y}$, and $\hat{z}$ are the efg principal axes; $V_{\hat{x}\hat{x}}$, $V_{\hat{y}\hat{y}}$, and $V_{\hat{z}\hat{z}}$ are the principal components of the efg. By convention $\hat{x}$, $\hat{y}$, and $\hat{z}$ are chosen so that $|V_{\hat{z}\hat{z}}| \geq |V_{\hat{y}\hat{y}}| \geq |V_{\hat{x}\hat{x}}|$. The ^{57}Fe nucleus in its $I = {}^1/_2$ ground state has no quadrupole moment and $\mathcal{H}_{Q^{1/2}} = 0$. If the effective magnetic field at the Fe nucleus is zero, the Mössbauer spectrum will be a quadrupole pair with splitting

$$\Delta E_Q = eQ\frac{V_{\hat{z}\hat{z}}}{2}(1 + \eta^2/3)^{1/2} \quad (3)$$

The zero-field spectrum of Ia is shown in Figure 7a; it consists of a quadrupole pair, as expected for an integer spin system. The quadrupole splitting $\Delta E_Q = 1.63$ mm/s is temperature independent for $T \leq 160$ K and the isomer shift δ at 4.2 K is 0.47 mm/s. The lines are broadened from the natural Lorentzian shape and have a width of 0.37 mm/s (full width at half-maximum). Figure 8a–e shows the field dependence of the Mössbauer spectra of Ia at 4.2 K. Spectra were also recorded in strong applied fields at temperatures between 10 and 160 K. At those temperatures intermediate electronic relaxation rates were observed and an analysis of those spectra will not be attempted here. However, the significant broadening observed at 4.2 K with $H^{app} = 0.06$ T (Figure 8a) proves that the relaxation rate at this temperature is close to the slow limit.

The broadening of the 0.06-T spectrum also suggests that an applied field of 0.5 T would saturate the electronic moment at least in one direction. The spectra in Figure 8c–e confirm this. Furthermore, the sharp lines of the 0.5-T spectrum indicate that the effective field, H^{eff}, is almost constant for all orientations of H^{app}, an indication of a very anisotropic induced electron moment. Given δ and ΔE_Q from the zero-field spectrum, we used the methods of Van Dongen Torman et al.[33] to identify possible combinations of H^{eff} and efg which yield the observed line positions. Solutions were found with $H^{eff} = 20.8 \pm 0.2$ T (along z), sign ($V_{\hat{z}\hat{z}}$) positive, $\hat{z}$ to be $12 \pm 2°$ from z, and $\eta = 0.4 \pm 0.1$. No solutions were found with the effective field close to the $\hat{x}\hat{y}$ plane. Within our spin Hamiltonian approximation such an anisotropic situation occurs for $D < 0$, $|D| > 2\beta_e H^{app}$, and $E/D < {}^1/_3$. The resulting ground doublet is predominantly $|S_z' = \pm 2\rangle$ and its zero-field splitting is given by

$$\Delta = 2|D|((1 + 3(E/D)^2)^{1/2} - 1) \quad (4)$$

For $H^{app} = 0.5$ T the electronic moment is essentially saturated along the z axis. At this point we chose **A** to be diagonal in the xyz frame, knowing that the quality of the final fits would de-

(33) J. Van Dongen Torman, R. Jagannathan, and J. M. Trooster, *Hyperfine Interact.*, **1**, 135 (1975).

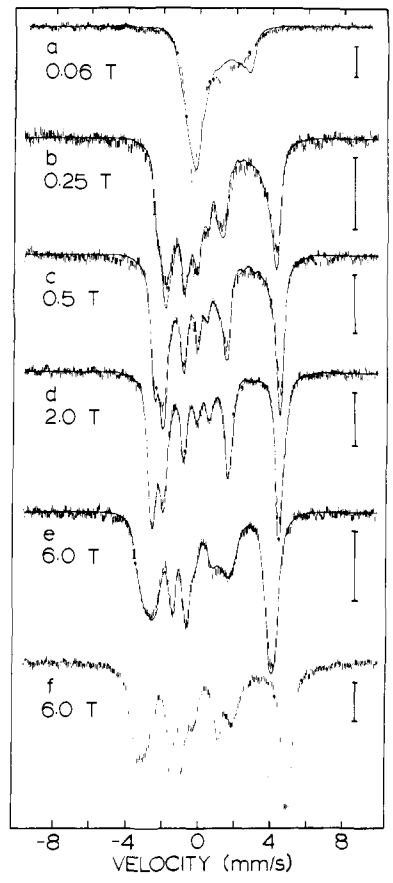

Figure 8. Mössbauer spectra of frozen DMF solutions of (a)–(e) $(Et_4N)_2[S_2MoS_2Fe(SPh)_2]$ and (f) $(Et_4N)_2[S_2MoS_2FeCl_2]$ recorded at 4.2 K and with applied parallel fields as indicated. The solid curves are theoretical simulations as described in the text. Vertical bars indicate 1% absorption.

termine the validity of this simplification. In the spin Hamiltonian formalism the effective field equals $H^{app} - (\mathbf{A}\cdot\hat{S})$ and, in this case, is governed primarily by Δ and A_z. Fitting the 0.06-, 0.25-, and 0.50-T spectra, we found $\Delta = 0.38$ cm^{-1} and $A_z = -11.0 \pm 0.2$ T.

The low-field spectra are relatively insensitive to D, A_x, A_y, and the directions of $\hat{x}$ and $\hat{y}$. However, the 6-T spectrum is sensitive to these parameters as the applied field is large enough to induce a significant electron moment in the xy plane. The values $D = -4$ cm^{-1}, $A_x = -22.0$ T, and $A_y = -18.5$ T with $\hat{z}$ in the yz plane and $\hat{y}$ along x yield a good fit to the 6-T data. (The zero-field splitting of 0.38 cm^{-1} implies $E/D = 0.18$.) These parameters should not be considered unique as a range of efg orientation, D, A_x, and A_y exists which will yield satisfactory fits. However, analysis of the 6-T data does show that D is between -3 and -6 cm^{-1} and that $\mathbf{A}$ is anisotropic with $A_x \simeq A_y$ and $A_z/A_x \lesssim 0.5$. The spin Hamiltonian parameters used to generate the solid curves in Figure 8 are listed in Table VII.

Mössbauer spectra of II dissolved in DMF were also recorded at several applied fields and temperatures. The gross features of the spectra are similar to those of Ia; the zero-field spectrum is shown in Figure 7b. The Mössbauer parameters of II are $\Delta E_Q = 2.12$ mm/s for $T \leq 160$ K and $\delta = 0.60$ mm/s for $T = 4.2$ K. The absorption peaks are very nearly Lorentzian with widths of 0.29 mm/s. As shown in Figure 8, the high-field spectra of Ia and II are almost identical and we may conclude that D, E/D, and $\mathbf{A}$ of these two complexes are also similar. Besides ΔE_Q and δ, other differences are discernible. Analysis of the 0.5-T data shows that $\hat{z}$ of II lies within 6° of z compared with 12° for Ia. Also II has poorer resolved features in applied fields <0.5 T which suggests that either Δ of II is larger than 0.38 cm^{-1} or that the electronic relaxation rate is not in the slow limit. The 4.2 K, 6-T spectrum is insensitive to Δ and the relaxation rate since $8\beta_e H \gg kT$ and $8\beta_e H \gg \Delta$.

Table VII. Fine and Hyperfine Parameters of $(Et_4N)_2[FeMoS_4(SPh)_2]$ and *C. pasteurianum* Rubredoxin

	$(Et_4N)_2$-$[S_2MoS_2Fe(SPh)_2]$	Cp Rd reduced[a]	Cp Rd oxidized[a]
S	2	2	5/2
D, cm^{-1}	−4.0	7.8	2.7
E/D	0.18	0.28	0.33
A_x, T	−22.0	−20.1	−16.5
A_y, T	−18.5	−8.3	−15.9
A_z, T	−11.0	−30.1	−16.9
δ, mm/s[b]	0.47	0.70	0.32
ΔE_Q, mm/s[b]	+1.63	−3.25	−0.50
η	0.4[c]	0.65	0.2
β, deg	12	*d*	*d*

[a] C. Shulz and P. G. Debrunner, *J. Phys. (Paris), Suppl.*, 12, C6-153 (1976). [b] At 4.2 K. [c] $\hat{y}$ along x. [d] Assumed to be zero.

Mössbauer Discussion. We now address the question of the distribution of the unpaired spin in Ia in terms of the Mössbauer results. For illustrative purposes, the fine and hyperfine parameters of Ia are listed in Table VII along with those of the reduced and oxidized forms of rubredoxin from *C. pasteurianum* (Cp Rd, ref 34). X-ray diffraction[35] and EXAFS[36] studies have shown that Cp Rd contains a single Fe site with tetrahedral sulfur coordination. The FeS_4 geometries of Cp Rd and Ia are very similar with the Fe–S bond distances in Cp Rd between 2.24 and 2.33 Å and its S–Fe–S angles between 104 and 115°. The observed isomer shift of Ia is atypical of either the ferrous or ferric ions and suggests more delocalization of the iron 3d electrons and/or an increased occupation of the 4s iron orbital relative to reduced Rd. The intermediate value of the quadrupole splitting of Ia should not be interpreted independently of the magnetic data. Similar quadrupole splittings and isomer shifts are observed for the $S = 1$, Fe^{2+} tetraphenylporphyrin (FeTPP, $\Delta E_Q = 1.51$ mm/s and $\delta = 0.52$ mm/s at 4.2 K, ref 37) and for two sites of the recently discovered 3Fe cluster of reduced ferredoxin II from *D. gigas*[38] and reduced ferredoxin I from *A. vinelandii* ($\Delta E_Q = 1.47$ mm/s and $\delta = 0.46$ mm/s at 4.2 K, ref 39). The iron site in the reduced 3Fe cluster may well be similar to that of Ia, but that of the FeTPP is very much different. Not only are the irons in different spin states and in drastically different chemical environments, but the observed efg of the FeTPP has been attributed[37] to nonvalence charges.

The magnetic hyperfine interaction allows us to make more definitive statements concerning the unpaired spins. Most important, the magnetic hyperfine interaction of Ia is anisotropic. As discussed by Kent et al.[40] the ratio $A_z/A_\perp = 0.5$ is characteristic of a high-spin ferrous ion with the sixth 3d electron occupying an oblate orbital. Below we use the perturbation expressions of Zimmermann et al.[41] to construct a crude model of $\mathbf{A}$ for a high-spin ferrous ion. A perturbation approach is reasonable since the temperature independence of ΔE_Q and the high temperature susceptibility indicate that the ground multiplet is well isolated. $\mathbf{A}$ may be written as

$$A_{pq} = [A^c + (g_p - 2)A^L]\delta_{pq} + A^d d_{pq} \qquad (5)$$

$$p, q = x, y, z$$

where A^c represents the isotropic Fermi contact contribution to $\mathbf{A}$, $(g_p - 2)A^L$ the orbital contribution, and $A^d d_{pq}$ the spin dipole

(34) C. Schulz and P. G. Debrunner, *J. Phys. (Paris), Suppl.*, **12**, C6-153 (1976).
(35) K. D. Watenpaugh, L. C. Sieker, and L. H. Jensen, *J. Mol. Biol.*, **131**, 509 (1979).
(36) B. Bunker and E. A. Stern, *Biophys. J.*, **19**, 253 (1977).
(37) G. Lang, K. Spartalian, C. A. Reed, and J. P. Collman, *J. Chem. Phys.*, **69**, 5424 (1978).
(38) B. H. Huynh, J. J. G. Moura, I. Moura, T. A. Kent, J. LeGall, A. V. Xavier, and E. Münck, *J. Biol. Chem.*, **255**, 3242 (1980).
(39) M. H. Emptage, T. A. Kent, B. H. Huynh, J. Rawlings, W. H. Orme-Johnson, and E. Münck, *J. Biol. Chem.*, **255**, 1793 (1980).
(40) T. A. Kent, K. Spartalian, and G. Lang, *J. Chem. Phys.*, **71**, 4899 (1979).
(41) R. Zimmermann, H. Spiering, and G. Ritter, *Chem. Phys.*, **4**, 133 (1974).

contribution. Freeman and Watson[42] have calculated $A^c = -27.5$, $A^L = 56.5$, and $A^d = 4.0$ T for the free ferrous ion. These values may be reduced by covalency effects but will suffice for our purposes. The orbital term arises from electron currents unquenched by spin–orbit coupling and, within our rough model

$$g_x = g_z - (2/\lambda)(D - E) \qquad g_y = g_z - (2/\lambda)(D + E) \quad (6)$$

where λ is the spin–orbit coupling constant and equals -103 cm^{-1} for the free ion.[41] The sign of the spin–orbit interaction is such that $g_p \geq 2$ and the orbital contribution to **A** opposes the contact contribution in all directions. The value and uncertainty of the observed μ_{eff} coupled with the large magnitude of A^L render calculations of the average orbital moment meaningless. Therefore, we simply choose the smallest g_p to equal 2 and proceed to the dipole term. The tensor d_{pq} is proportional to the valence efg, V_{pq}^{val}, with sign (d_{pq}) = sign (V_{pq}^{val}). The quantity $d = d_{zz}(1 + \eta_{val}^2/3)^{1/2}$ will equal ± 2 if the orbital moment is totally quenched. Assuming that the observed efg is proportional to the valence efg and that $d = 2$, we use the D, E/D, and efg of Table VII and calculate from eq 5 $A_x = -20$, $A_y = -11$, and $A_z = -35$ T for reduced Cp Rd and $A_x = -31$, $A_y = -30$, and $A_z = -15$ T for Ia. Comparison with the observed values shows that our crude high-spin ferrous model accounts for the anisotropy of **A** for both Cp Rd and Ia. In contrast, the **A** of high-spin ferric ions are dominated by the contact term with all the A_i typically being within 15% of their average. Hence, the Mössbauer data suggest that the $[S_2MoS_2Fe(SPh)_2]^{2-}$ cluster is more accurately described as $Fe^{2+}Mo^{6+}$ rather than $Fe^{3+}Mo^{5+}$. The small quadrupole splitting and isomer shift of Ia do raise questions concerning the extent of the delocalization of some or all of the iron 3d electrons. However, we hesitate to draw any conclusions concerning this point since the present uncertainty in the orbital term prevents any quantitative comparison of the **A** of Ia with those of other complexes.

A simple linear relationship of isomer shift to average oxidation state has been established for iron in tetrahedral sulfur environments.[6b] For Ia we have observed an isomer shift of 0.43 mm/s at 160 K and estimate $\delta = 0.45$ mm/s at 77 K. After subtracting 0.12 mm/s to correct for our 300 K source temperature, we find that Figure 7 of ref 6b predicts an effective oxidation state of +2.6. However, the similarity of the isotropic parts of **A** for Ia and reduced Rd plus the anisotropy discussed above suggest a more ferrous character. We conclude that a definitive assignment of oxidation state to iron in mixed iron–molybdenum complexes such as Ia is difficult at best and that a simple relationship of isomer shift to such an assignment may not exist.

(42) A. J. Freeman and R. E. Watson, *Phys. Rev.*, **131**, 2566 (1963).

Conclusions

The heterobimetallic species $[S_2MoS_2FeX_2]^{2-}$ (X = Cl, aryl thiolate) are readily prepared and interconverted. Analysis of magnetic susceptibility and Mössbauer data suggests a high-spin Fe(II)–Mo(VI) formulation. The dimensions and chemical reactivity of the MoS_2Fe core are comparable to those found in complexes containing the Fe_2S_2 core. Most importantly, the MoS_2Fe unit exhibits a stability comparable to that of the $MoFe_3S_4$ substituted cubane, and thus must also be considered as a potential structural fragment in the FeMo cofactor of nitrogenase.

Acknowledgments. This research was supported by grants to B.A.A. from the National Science Foundation (CHE-7715990) and the USDA/SEA Competitive Research Grants Office (5901-0410-8-0175-0) and by grants to E. Münck from the National Science Foundation (PCM77-08522) (T.A.K.) and the National Institutes of Health (GM22701) (B.H.H.). H.C.S. was supported by a General Electric Co. Summer Fellowship (1979). We thank E. Bouhoutsos-Brown for assistance with the NMR spectra and E. Münck for helpful discussions. We are grateful to Dr. F. J. DiSalvo at Bell Laboratories for assistance with and discussions on the temperature-dependent susceptibility data.

Supplementary Material Available: Positional and thermal parameters (Table VIII), interatomic distances (Table IX), and bond angles (Table X) for the cations (3 pages). Ordering information is given on any current masthead page.

Phosphorus-31 Spin–Lattice Relaxation in Aqueous Orthophosphate Solutions[1]

Douglas C. McCain*[2] and John L. Markley

Contribution from the Department of Chemistry, Purdue University, West Lafayette, Indiana 47907. *Received February 14, 1980*

Abstract: Phosphorus-31 spin–lattice relaxation rates and nuclear Overhauser enhancements were measured for sodium orthophosphate in aqueous solution as a function of pH, temperature, concentration, magnetic field strength, and percent deuterium in the solvent. We demonstrate that relaxation easily can be dominated by trace impurities of transition-metal ions. In rigorously purified samples, the longitudinal relaxation rate is nearly independent of pH or concentration. The longitudinal relaxation rate has been resolved into contributions from dipole–dipole, chemical shift anisotropy, and residual components. The results support an ion–solvent interaction model in which the PO_4 group is locked into the local water structure by numerous hydrogen bonds. We propose a hydrogen-bond shift mechanism, termed "quasi-rotation", which accounts for the observed chemical shift anisotropy relaxation rate. Proton tunneling appears to influence chemical shift anisotropy relaxation in H_2O but not in D_2O at low temperatures. We suggest that the residual relaxation component which has a positive activation energy arises from "quasi-spin rotation" resulting from hydrogen-bond shifts.

Introduction

Phosphorus-31 nuclear spin relaxation in aqueous orthophosphate solutions has been the subject of several publications.[3-9] Some of the literature data have been replotted in Figure 1 as ^{31}P spin–lattice relaxation rates, $1/T_1$, vs. pH. There is general

(1) Presented at the Great Lakes Regional Meeting of the American Chemical Society, Rockford, Ill., June 1979.

(2) Department of Chemistry, Southern Station Box 9281, University of Southern Mississippi, Hattiesburg, Miss. 39401.

(3) W. E. Morgan and J. R. Van Wazer, *J. Am. Chem. Soc.*, **97**, 6347 (1975).

0002-7863/80/1502-5559$01.00/0